*ISSN 1027-4510, Journal of Surface Investigation. X-ray, Synchrotron and Neutron Techniques, 2012, Vol. 6, No. 4, pp. 623–630. © Pleiades Publishing, Ltd., 2012.*
*Original Russian Text © A.E. Galashev, 2012, published in Poverkhnost'. Rentgenovskie, Sinkhrotronnye i Neitronnye Issledovaniya, 2012, No. 7, pp. 80–88.*

# Physical Properties of Silver-Coated Silica Clusters: A Computer Experiment

**A. E. Galashev**
*Institute of Industrial Ecology, Ural branch, Russian Academy of Sciences, Ekaterinburg, Russia*

Received July1, 2011

**Abstract**—The effect on the physical properties of a silica cluster after silver coating has been studied by the molecular dynamics method. It has been established that silver atoms make a sphere-like cluster shape, increase mechanical stability and give a stable positive value of the surface tension. They increase the number of electrons able to interact with the electromagnetic field, and, hence, enhance the efficiency of thermal radiation transfer by clusters.

**DOI:** 10.1134/S1027451011120056

## INTRODUCTION

Self-organization is a fundamental mechanism, by means of which microstructures are transformed into the elements of nanomaterials. Atoms, molecules, macromolecules, as well as colloidal particles are involved in the process of building elements or blocks of nanomaterials. It is known that the same chemical compound may have absolutely different physical properties depending on how its “building” blocks were formed. For example, the organization of carbon atoms in a diamond structure creates the hardest mineral on Earth, while a graphite structure is easily separated layer by layer (a graphite pencil leaves a trace without significant effort). The difference of the properties of these materials is in the manner of the carbon atom stacking. Structures on the nanometer scale, as a rule, are created not for obtaining materials with high hardness, but rather for the optical properties inherent to them. When obtaining new nanomaterials, it is important to know how self-organization of their structure occurs. Usually, self-organization occurs in a narrow interval of the particle sizes. There are a limited number of materials, for which monodisperse colloidal particles are easily synthesized. Silicon dioxide belongs to such materials [1]. Materials obtained by the deposition of gold or silver on silica particles are rather promising.

Much effort was put into obtaining a new class of materials by modification of the surface structure of nanoparticles. In addition to the highly developed surface, such particles have physical and chemical properties, which differ from those of three-dimensional phases and individual molecules. They demonstrate potential applicability in optics, optoelectronics, color diagnostics, photothermal therapy, catalysis etc. A strong interaction of light with precious-metal nanostructures appears at frequencies close to the resonance frequency of the plasmon present in these particles. The metal nanoparticles give the effect of enhanced fluorescence. The silver-coated nanoparticles, as well as the silver island films produce higher (up to 100 times) luminescence in dying materials in comparison with the situation, when these compounds are on a simple glass substrate.

In a liquid state the $SiO_2$ is vitrescent. Liquids of such a type are conventionally classified according to the low-temperature behavior of viscosity $\eta$ [2, 3]. The frailty of glass is characterized by the index $m$, which reflects the degree of the deviation of the liquid's viscosity from the Arrhenius behavior in the vitrification region and can be determined as follows [4]:

$$m = \left[\frac{1}{2.303}\frac{d\ln\tau}{d(T_g/T)}\right]_{T - T_g} = \left[\frac{d\log(\eta)}{d(T_g/T)}\right]_{T = T_g}, \qquad (1)$$

where $\tau$ is the relaxation time of the shift stress, $T_g$ is the temperature of the vitrification transition.

The stronger the dependence of $\log(\eta)$ on $T_g/T$ deviates from the linear, the higher index $m$ is and the frailer(short-lived) the glass is. The strong liquids are characterized by a linear behavior of this function, i.e., small values of index $m$. In this case the Arrhenius behavior of viscosity is observed, i.e., $\ln\eta \sim 1/T$. Liquid silicon dioxide is a “strong” liquid. The transition of this liquid into a “frail” state occurs at a high temperature (~4000 K) and high density [5].

Recently, composite materials built by way of the introduction of metal nanoclusters into a quartz matrix have attracted a great deal of attention. These materials are planned to be used in optical and optoelectronic devices [6]. Their use in integrated optics and waveguides is based on their high sensitivity to the excitation of the surface plasmon of nanosize metal particles [7]. It has been shown that small silver clusters consisting of only several atoms have intriguing properties, and their fluorescence is an ideal instru-

Parameters of potentials

| Parameter | $q_{\mathrm{O}}$, $e$ | $q_{\mathrm{Si}}$, $e$ | $q_{\mathrm{Ag}}$, $e$ | $\alpha^{(p)}_{\mathrm{SiO_2}}$, Å$^3$ | $\sigma^{LJ}_{\mathrm{Ag-Si}}$, nm |
|---|---|---|---|---|---|
| Value | −1.38257 | 2.76514 | 0 | 3.219 | 0.339 |
| Parameter | $\chi_{\mathrm{O-O}}$ | $\chi_{\mathrm{Si-O}}$ | $\chi_{\mathrm{Si-Si}}$ | $\chi_{\mathrm{Ag-Ag}}$ | $\sigma^{LJ}_{\mathrm{Ag-O}}$, nm |
| Value | 12.07092 | 11.15230 | 10.45517 | 8.52887 | 0.285 |
| Parameter | $B_{\mathrm{O-O}}$, kJ/mole | $B_{\mathrm{Si-O}}$, kJ/mole | $B_{\mathrm{Si-Si}}$, kJ/mole | $B_{\mathrm{Ag-Ag}}$, kJ/mole | $\varepsilon^{LJ}_{\mathrm{Ag-Si}}$, kJ/mole |
| Value | 0.32830 | 2.52487 | 2.76538 | 32.06025 | 20.55611 |
| Parameter | $r^0_{\mathrm{O-O}}$, nm | $r^0_{\mathrm{Si-O}}$, nm | $r^0_{\mathrm{Si-Si}}$, nm | $r^0_{\mathrm{Ag-Ag}}$, nm | $\varepsilon^{LJ}_{\mathrm{Ag-O}}$, kJ/mole |
| Value | 0.37942 | 0.24538 | 0.30429 | 0.31150 | 4.56498 |

ment for fundamental studies, allowing one to determine their atomic and electronic structure [8, 9]. Small-size silver clusters in a matrix of annealed quartz were obtained in [10]. Such clusters were acidized for several weeks leading to the disappearance of the plasmon resonance. Such resonance was observed in optical absorbers, thin $SiO_2$ films with a high concentration of silver clusters grown from silver nitrate absorbed by the film [11]. Silver particles coated by the $SiO_2$ film demonstrate an optical restriction when under the action of a nanosecond pulse with a wavelength of 532 nm [12]. The $SiO_2$ protects the particle from laser destruction. Thus, the material obtained from these particles can create an optical restriction at high-energy irradiation.

The surface tension $\gamma$ is considered as an important factor in the stabilization of the small particles and clusters. However, it is not easy to determine the $\gamma$ for systems, which have a curved surface, in atomic scale calculations. Up to now there is no strictly established way of calculating $\gamma$ for clusters, particularly, when they are found in the solid state and have large internal stresses [13]. Surface tension is one of the factors, controlling the change of the morphology, determined by the catalytic annealing of nanoparticles [14]. The experimental surface tension of the solid state is determined by the contact angle, formed at the boundary with the liquid, the surface tension of which is known [15]. In this case the $\gamma$ for the liquid serves as a reference. For many metals in the region of $d > 1$ nm the dependence $\gamma(d)$ disappears [16]. The $d > 1$ nm Ag nanoparticles are characterized by a surface tension, estimated by the values from the range $1.415 \le \gamma \le 6.56$ n/m [17–22]. Such scatter in the $\gamma$ is explained by the effect of the surroundings (most often the substrate). The effect of the surroundings on the $\gamma$ value can be completely eliminated in the computer experiment.

The aim of this work is to study the structure formation of silver-coated silica clusters, and to determine the physical properties of such clusters, including the surface tension, depending on the number of adsorbed silver atoms.

## MOLECULAR-DYNAMIC MODEL

To describe the pair part of the interactions in the $SiO_2$ system, the Coulomb potential and the Morse potential are used [23]:

$$\Phi(r_{ij}) = \frac{q_i q_j}{r_{ij}} + B_{ij}\left[\exp\{\chi_{ij}[1 - r_{ij}/r^0_{ij}]\} - 2\exp\left\{\frac{\chi_{ij}}{2}[1 - r_{ij}/r^0_{ij}]\right\}\right], \tag{2}$$

where the interaction between an atom of the $i$ type and an atom of the $j$ type is determined by the parameters $q_i$, $q_j$, $B_{ij}$, $\chi_{ij}$, $r^0_{ij}$ (table) and distance between them $r_{ij}$. This potential was cut at a distance of 0.9 nm. The effects of dipolar polarization were included in addition to the pair potential. The polarizability $\alpha^{(p)} = 3.219$ Å, corresponding to the experimental value of the polarizability of $SiO_2$ molecules, was referred to the Si nucleus of this structural unit. The Si–O distance in the structural unit corresponded to the smallest distance $r_{\mathrm{Si-O}} = 0.162$ nm in the quartz crystal, and the angle O–Si–O was taken to equal the tetrahedral angle 109.5°.

The description of the interaction between silver atoms in the model is based on the use of the Morse potential [24]. The parameters of this potential are given in the table. The atom–atom Si–Ag and O–Ag interactions were given by the Lennard–Jones potential with the parameters $\sigma^{LJ}$ and $\varepsilon^{LJ}$, taken from [25]. The values of these parameters are also given in the table.

Flexible models of the "molecules" were considered. The flexibility of "molecules" was provided on account of the procedure, elaborated within the Hamilton dynamics of [26, 27]. Let us consider a two-atomic molecule. Let $a$ and $b$ atoms in the molecule be separated by the distance

$$u = \|\mathbf{r}_a - \mathbf{r}_b\|, \tag{3}$$

where $\mathbf{r}_a$ and $\mathbf{r}_b$ are vectors, determining the positions of the atoms. Let us denote the corresponding to velocities as $\mathbf{v}_a$ and $\mathbf{v}_b$, and the reduced mass we write as

$$\mu = \frac{m_a m_b}{m_a + m_b}. \tag{4}$$

The size of the molecule, presented by the atoms $a$ and $b$, is determined by equilibration of the complete potential force $\mathbf{f}(\mathbf{u}) = -\frac{\partial \mathbf{r}}{\partial \mathbf{u}} \nabla\Phi(\mathbf{r})$ by the centrifugal force $-\mu u \omega^2$ so that

$$-\mu u \omega^2 - \nabla\Phi(\mathbf{r})\frac{\partial \mathbf{r}}{\partial \mathbf{u}} = 0, \tag{5}$$

where $\omega = \|\mathbf{v}_a - \mathbf{v}_b\|/u$ is the angular velocity. By using the minimization contribution to the potential energy $U$ from each of the generalized coordinates, we obtain:

$$\frac{\partial}{\partial u_i} H(\mathbf{r}, \mathbf{v}) = \frac{\partial}{\partial u_i}\left(\frac{1}{2}\mu_i u_i^2 \omega_i^2 + U(\mathbf{r})\right) = 0. \tag{6}$$

This method is generalized to the molecules of any composition [28].

The initial packing of the $SiO_4$ tetrahedra, presenting the nanoparticle of $(SiO_2)_{50}$ quartz, was obtained by means of the GRINSP computer program [29]. The structural $SiO_2$ units were separated in this packing. The initial velocities of the $SiO_2$ particles were set in a random manner; they were adjusted to a temperature of 293 K by dividing the input or output thermal energy proportionally to the velocity. Then the preliminary molecular-dynamic (MD) calculation for 50 structural $SiO_2$ units united in a cluster was performed. The duration of this calculation was one million time steps, with the value of a step being $\Delta t = 10^{-16}$ s. During this period the studied system reached an equilibrium state as indicated by the establishment of the Maxwell distribution of velocities of the $SiO_2$ objects. Meanwhile, the structure of the nanoparticles relaxed to the energy-advantageous packing ($U \approx -0.9$ eV/freq). Then, at the time moment, taken as zero ($t = 0$), silver atoms were introduced into the environment of the $(SiO_2)_{50}$ nanoparticle. Determination of the location of the Ag atoms was performed by means of the virtual face-centered cubic (FCC) lattice, penetrating the $(SiO_2)_{50}$ cluster. The lattice constant was 0.6 nm. The lattice sites nearest to the silica nanoparticle which were located at a distance no less than 0.6 nm from each Si or O atom were determined. These sites were filled with silver atoms. Three calculations were performed with different numbers $N_{Ag}$ of silver atoms surrounding the $(SiO_2)_{50}$ nanoparticle: $N_{Ag} = 10$, 30 and 50. In each case the main calculation was preceded by a preliminary calculation with a duration of $0.5 \times 10^6\ \Delta t$, during which the necessary structural relaxation of the system took place. The main calculation for the determination of the spectral features of the systems, consisting of the $(SiO_2)_{50}$ cluster in the surrounding of Ag atoms, was $2.5 \times 10^6\ \Delta t$.

The fourth-order Gear method [30] was used to integrate the equations of motion of the mass centers of the $SiO_2$ structural units and Ag nuclei. The analytical solution of the equations of motion for the rotation of the structural units was implemented with the use of the Rodrigues–Hamilton parameters [31], and the integration scheme of equations of motion in the presence of rotations corresponded to the approach proposed by Sonnenschein [32].

The method of calculation of the complex dielectric permeability $\varepsilon(\omega) = \varepsilon'(\omega) - i\varepsilon''(\omega)$ is given in [33, 34]. The total number of electrons $N_{el}$ in the volume unit of the cluster, interacting with the external electromagnetic field, is given as [35]:

$$N_{el} = \frac{m}{2\pi^2 e^2}\int_0^\infty \omega\varepsilon''(\omega)d\omega, \tag{7}$$

where $e$, $m$ are the charge and mass of the electron, respectively.

The calculations were performed on a PENTIUM-IV four-nucleus computer with a processor tact frequency of 2.83 GHz.

## CLUSTER SURFACE TENSION

The pressure tensor for a droplet (cluster) in the spherical coordinates can be presented as

$$\mathbf{p}(\mathbf{r}) = p_N(r)[\mathbf{e}_r\mathbf{e}_r] + p_T(r)[\mathbf{e}_\theta\mathbf{e}_\theta + \mathbf{e}_\phi\mathbf{e}_\phi], \tag{8}$$

where $\mathbf{e}_r$, $\mathbf{e}_\theta$ and $\mathbf{e}_\phi$ are the orthogonal unit vectors, and $p_N(r)$ and $p_T(r)$, representing the normal and transverse components of the pressure tensor, are functions of the distance $r$ from the center of the cluster masses.

The Irving–Kirkwood pressure tensor was calculated in the approximation of a spherically symmetrical system by the method described in [36]. At the calculation of the surface tension $\gamma$ the contributions of $n$ stressed concentric layers, in which the cluster is split, are summed. Let us write the normal component $p_N(r)$ as the sum of the kinetic and configuration contributions:

$$p_N(r) = p_K(r) + p_U(r), \tag{9}$$

where $p_K(r) = kT\rho(r)$, $\rho(r)$ is the density profile. The configuration term is determined as

$$p_U(r) = S^{-1}\sum_k f_k, \tag{10}$$

where $4\pi r^2$ is the area of the spherical surface of the radius $r$, and the sum over $k$ is the sum of the normal components $f_k$ of all pair forces, acting through the surface. The values of the force $f_k$ are scalar; they are

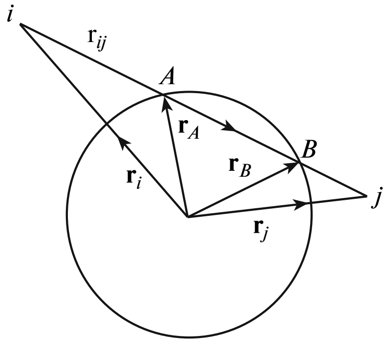

**Fig. 1.** Geometric representation of the method of calculation of the contribution to the pressure tensor of a pair of molecules $i$ and $j$, between which surface $S_i$ is twice cut by the distance $r_{ij}$.

positive for repulsion forces and negative for attraction forces. The scheme of the calculation of their contribution for a unit surface $S_1$ and one pair of atoms is shown in Fig. 1. The vector of the force of the quantity $f(r_{ij})$ acts along the radius $\mathbf{r}_{ij} = \mathbf{r}_j - \mathbf{r}_i$ and crosses $S_1$ at two points $A$ and $B$. These points are localized on the ends of vectors $\mathbf{r}_A$ and $\mathbf{r}_B$. Depending on the location of atoms $i$ and $j$, there can be one intersection as well. Two possible calculated normal components are the same due to symmetry. Let us study one of these points and denote the vector characterizing it as $\mathbf{r}$. The force vector is given as

$$\mathbf{f}(\mathbf{r}_{ij}) = \hat{\mathbf{r}}_{ij} f(r_{ij}) = -\hat{\mathbf{r}}_{ij}\frac{\mathrm{d}\Phi(r_{ij})}{\mathrm{d}r_{ij}}, \tag{11}$$

where $\hat{\mathbf{r}}_{ij}$ is the unit vector, directed along $\mathbf{r}_{ij}$, and corresponding to the term $f_k$ is determined as

$$f_k = |\hat{\mathbf{r}} \cdot \hat{\mathbf{r}}_{ij}| f(r_{ij}) = |\mathbf{r} \cdot \mathbf{r}_{ij}| f(r_{ij})/rr_{ij}, \tag{12}$$

So that

$$p_U(r) = -(4\pi r^3)^{-1}\sum_k |\mathbf{r} \cdot \mathbf{r}_{ij}| \frac{1}{r_{ij}}\frac{\mathrm{d}\Phi(r_{ij})}{\mathrm{d}r_{ij}}. \tag{13}$$

Since the end of the vector $\mathbf{r}$ rests upon $S_1$ and is between $i$ and $j$, it is possible to write

$$\mathbf{r} = \frac{1}{2}(r_i + r_j + \xi r_{ij}), \tag{14}$$

where $\xi$ is a not yet determined constant from the interval

$$-1 \le \xi \le +1. \tag{15}$$

For the given $(i, j)$ pairs there can be intersections with several surfaces depending on the selected distance between them. Thus, it is necessary to determine the maximum and minimum distances of the vector $\mathbf{r}_{ij}$ from the center of the cluster mass in order to determine, what surfaces have $f_k$ – contributions from the given pair of atoms. The maximum distance is obviously set as

$$r_{\max} = \max(r_i, r_j), \tag{16}$$

where it is possible to find values $\xi$, $\xi_{\min}$, which characterize the minimum distance $r_{\min}$ by minimizing the square of expression Eq. (14) with respect to $\xi$. The results of this are:

$$\xi_{\min} = \frac{r_i^2 - r_j^2}{r_{ij}^2} \tag{17}$$

and

$$r_{\min} = \begin{cases} \dfrac{1}{2}\left[2(r_i^2 + r_j^2) - r_{ij}^2 - \dfrac{(r_i^2 + r_j^2)^2}{r_{ij}^2}\right]^{1/2}, & |\xi_{\min}| \le 1, \\ \min(r_i, r_j), & |\xi_{\min}| > 1. \end{cases} \tag{18}$$

For each of the two possible crossings of the different surfaces, being between the level $r_{\min}$ and $r_{\max}$, different $\xi$ values correspond to the given pair$(i, j)$. It is possible to find two values $\xi$ for the given surface, i.e., $\xi_+$ and $\xi_-$, by squaring expression Eq. (14) and solving the obtained quadratic form. The result is:

$$\xi_\pm = \frac{r_i^2 - r_j^2}{r_{ij}^2} \pm \left[\left(\frac{r_i^2 - r_j^2}{r_{ij}^2}\right)^2 + 1 - 2\left(\frac{r_i^2 + r_j^2}{r_{ij}^2}\right) + \frac{4r^2}{r_{ij}^2}\right]^{1/2} \tag{19}$$

and, since for both intersections the scalar product, appearing in Eq.(13), has the same value (as required by symmetry),

$$|\mathbf{r} \cdot \mathbf{r}_{ij}| = \frac{1}{2} r_{ij}^2 \left[\left(\frac{r_i^2 - r_j^2}{r_{ij}^2}\right)^2 + 1 - 2\left(\frac{r_i^2 + r_j^2}{r_{ij}^2}\right) + \frac{4r^2}{r_{ij}^2}\right]^{1/2}. \tag{20}$$

If either $|\xi_+| > 1$, or $|\xi_-| > 1$, then there is only one intersection. If $|\xi_+| \le 1$ and $|\xi_-| \le 1$, then there are two intersections.

The time spent on calculations is not independent of the chosen separating surfaces, since here there is a cycle over the surfaces (from $r_{\min}$ to $r_{\max}$) within the cycle over pairs of particles. Therefore too high a resolution leads to an increase in the calculation time, and an increase in the distance between surfaces does not improve the statistics. There is a reasonable compromise related to the use of $\Delta r \sim 0.1\sigma^{LJ}$.

The general condition of the mechanical equilibrium leads to the expression

$$p_T(r) = p_N(r) + \frac{r}{2}\frac{\mathrm{d}p_N(r)}{\mathrm{d}r}. \tag{21}$$

On the basis of the conditions of the mechanical equilibrium for the force and rotational moment on a hypothetical narrow cut surface of the droplet, Becker [37] and Buff [38] obtained the equation

$$\gamma = \int_0^\infty \left(\frac{r}{R_s}\right)^2 [p_N(r) - p_T(r)]\mathrm{d}r. \tag{22}$$

## RESULTS OF THE CALCULATION

Configurations of the $Ag_{50}(SiO_2)_{50}$ cluster, referring to the time moments of 0 and 250 ps, are shown in Fig. 2. The $SiO_2$ aggregate had the structure of

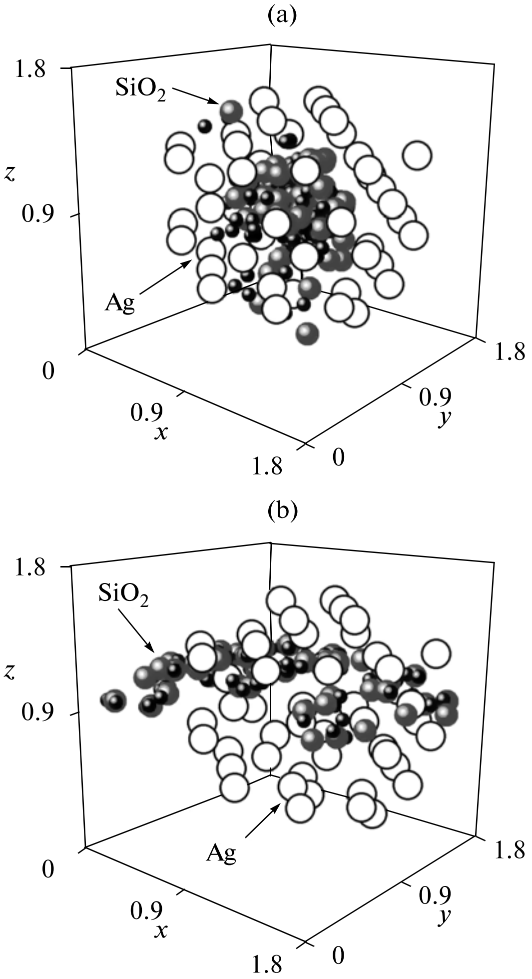

**Fig. 2.** Configurations of the $Ag_{50}(SiO_2)_{50}$ cluster, corresponding to time moments 0 (a) and 250 ps (b) (the atomic coordinates are given in nanometers).

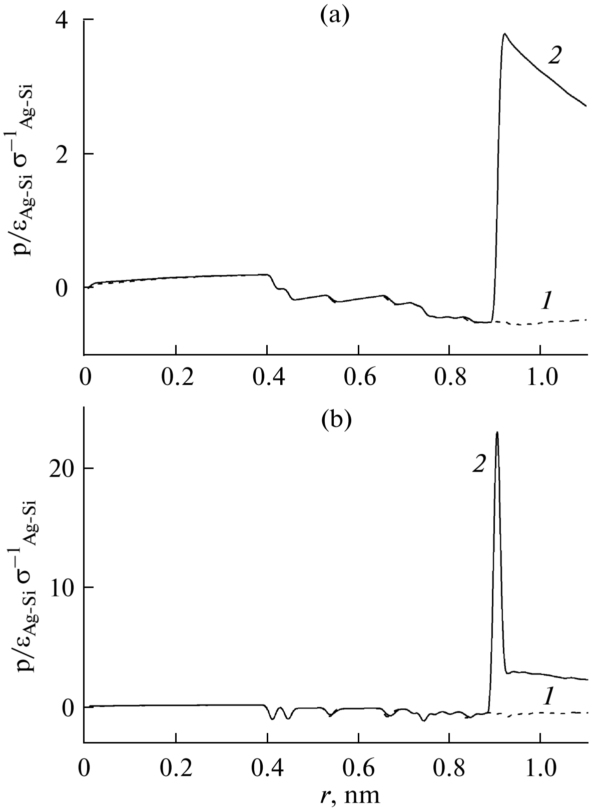

**Fig. 3.** Normal (a) and tangential (b) components of the pressure tensor for clusters: (1) $(SiO_2)_{50}$, (*2*) $Ag_{50}(SiO_2)_{50}$.

α-quartz in the initial state and the adsorbed Ag atoms were situated in the sites of the imaginary FCC lattice so that the $r_{O-Ag}$ and $r_{Si-Ag}$ distances did not exceed the values specified above. It is seen that the interaction with the Ag atoms did not hamper the formation of the $SiO_2$"crust". The "crust" is of the form of connected islands. In turn, the presence of the $SiO_2$ "crust" did not affect the formation of a fragment with a spherical form made from silver atoms. The Ag atoms are in close contact with the Si and O atoms, filling the gaps between the $SiO_2$ structural units. The internal part of the silver cluster, in contact with the "crust", is disordered. However, the crystalline ordering inherited from the initial FCC packing of the Ag atoms is traced to the periphery. The observed structural relaxation was mainly related to the displacement of more light and mobile $SiO_2$ structural units.

The radial distributions of the normal $p_N$ and tangential $p_T$ components of the pressure tensor for $(SiO_2)_{50}$ and $Ag_{50}(SiO_2)_{50}$ clusters are shown in Fig. 3. It is seen that up to distances of ~0.88 nm the $p_N(r)$ and $p_T(r)$ functions, corresponding to clusters of any type, have close values. However at larger distances the values of these functions differ considerably. At $r > 0.88$ nm the $p_N(r)$ function for the $Ag_{50}(SiO_2)_{50}$ cluster takes only positive values, and the values of the $p_T(r)$ function for this cluster can be both positive and negative. Such behavior of the $p_N(r)$ and $p_T(r)$ functions indicates that stresses in the internal part of the cluster, initially formed by the $SiO_2$ structural unit, change little after the adsorption of silver by the cluster, and the considerable enhancement of the stresses affected only the cluster surface, i.e., the region where the Ag atoms are mainly concentrated. The $p_N(r)$ and $p_T(r)$ profiles for the clusters with 10 and 30 silver atoms are close to the corresponding profiles of the $Ag_{50}(SiO_2)_{50}$ cluster.

The method used for the calculation of the surface tension assumes the presentation of the cluster in the form of a sphere, separated into concentric layers. The radius of the sphere (cluster) corresponded to the distance from the center of the cluster masses to the center of the most remote structural unit or nucleus of the atom. The partition was performed for 24 concentric layers of the same thickness $r \approx 0.13\sigma^{LJ}_{Ag-Si}$. The values of radius $R_s$ of the tension surface determined by the condition $d\gamma/dr = 0$, are shown in Fig. 4. It is seen that

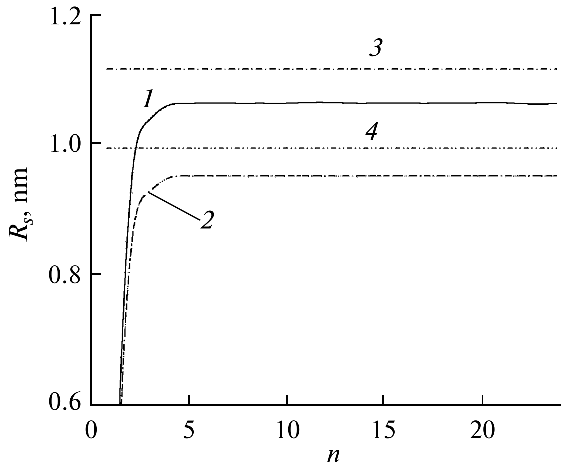

**Fig. 4.** Radius of the tension surface (*1*, *2*) depending on the number of concentric layers *n* used for the determination of the surface tension; (*3*, *4*) – effective cluster radius; (*1*, *3*) $(SiO_2)_{50}$, (*2*, *4*) $Ag_{50}(SiO_2)_{50}$. Layer numbering begins from the center of the mass of the cluster.

radius $R_s$ decreases after the adsorption of the Ag atoms by the $(SiO_2)_{50}$ cluster. The $R_s$ value became smaller by 10% in all three cases, i.e., after the adsorption of 10, 30 and 50 Ag atoms. The $R_s$ value takes the constant value already at $n = 5$ in the dependence $R_s(n)$, where *n* is the number of concentric layers with the beginning of the numbering from the center of the cluster masses. The radius of the tension surface is 4–5% less than the cluster radius.

The dependences $\gamma(n)$ for the $(SiO_2)_{50}$ clusters differ considerably with and without the Ag atoms (Fig. 5). In the absence of silver atoms, the $\gamma$ is negative and in the presence of Ag atoms, the $\gamma$ values are positive. The negative $\gamma$ values indicate the instability of the form of the aggregate that was completely confirmed in the calculation process. By the time moment 250 ps the sphere-like $(SiO_2)_{50}$ cluster took the form of a curved film, while the clusters with Ag atoms remained sphere-like. The small difference between the $\gamma$ values $\gamma$ for clusters, containing 10, 30 and 50 Ag atoms, agrees with the conclusion of [16] that the plateau of the dimensioned dependence of the $\gamma$ value for silver clusters is reached fast. The horizontal lines *5* and *6* in the figure show the experimental $\gamma$ values for silver nanoparticles [19] and Ag-nanowires [39], respectively. On average, the deviation of the calculated $\gamma$ values from the experimental value of the surface tension of silver nanoparticles [19] is no more than 13.4%, indicating the adequacy of the model we used.

The behavior of the $\gamma$ value depending on the number of Ag atoms in the cluster (curve *1*) is shown in Fig. 6. It was enough to have ten adsorbed Ag atoms for the $\gamma$ value to become positive (1.55 n/m). At $i > 10$ the dependence $\gamma(i)$ is close to linear. An increase in the number of silver atoms in the cluster from 10 to 30 leads to an increase in the value of the surface tension by 4.9%. The transition from $i = 30$ to $i = 50$ is accompanied by an increase in the $\gamma$ value of 4.7%. The line *2* in the figure shows the experimental $\gamma$ value for silver nanoparticles with an average size of 3.9 nm, placed in the silicate glass, consisting of $SiO_2$ at 71.9% [40]. The $\gamma$ values we obtained for $Ag_i(SiO_2)_{50}$ clusters ($i \geq 10$) agree with the experimental data within 8% of the average [40]. However, here the difference in the surrounding of the model and experimental nanoparticles should be taken into consideration. The calculated $\gamma$ value for $(SiO_2)_{576}$ nanoparticles at a temperature of 1500 K is shown by line *3* [41]. The $\gamma$ value for silica nanoparticles is 47% below the average $\gamma$ value for $Ag_i(SiO_2)_{50}$ clusters, $i \geq 10$.

The silica cluster with 30 Ag atoms turns out to be the most stable in accordance with the mechanical criterion of stability $(1/V\beta_T > 0)$, where *V* is the volume,

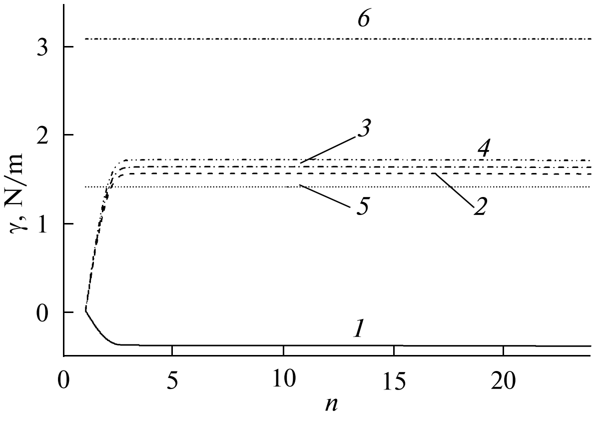

**Fig. 5.** Surface tension depending on the number of concentric layers used for its determinations for clusters: (*1*) $(SiO_2)_{50}$, (*2*) $Ag_{10}(SiO_2)_{50}$, (*3*) $Ag_{30}(SiO_2)_{50}$, (*4*) $Ag_{50}(SiO_2)_{50}$; (*5*) $\gamma$ value for silver nanoparticles, experiment [19], (*6*) $\gamma$ value for Ag nanowires, experiment [39].

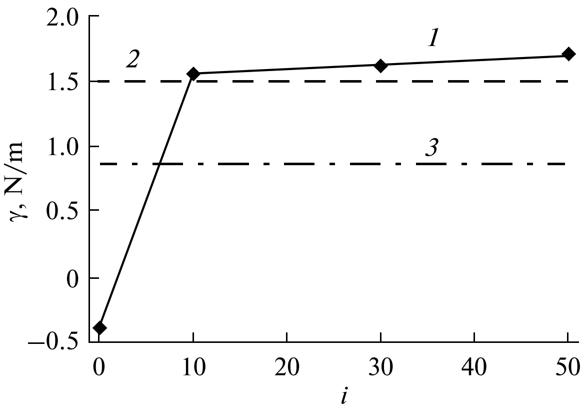

**Fig. 6.** Surface tension depending on the number *i* of Ag atoms in the cluster: (*1*) $Ag_i(SiO_2)_{50}$ clusters, present calculation; (*2*) silver nanoparticles in silicate glass, experiment [40]; (*3*) $(SiO_2)_{576}$ nanoparticles, MD-calculation [41].

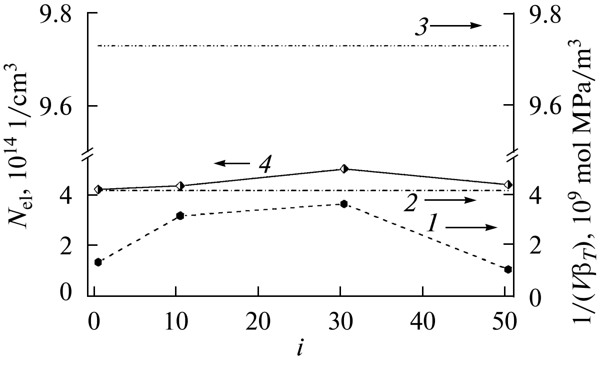

**Fig. 7.** Dependences of: (*1*) the mechanical stability coefficient $1/V\beta_T$, (*4*) – number of electrons interacting with the external electromagnetic radiation, on the number of silver atoms in $Ag_i(SiO_2)_{50}$ clusters; (*2*) mechanical stability coefficient of α-quartz, experiment [43]; (*3*) coefficient $1/V\beta_T$ of crystalline silver, experiment [44].

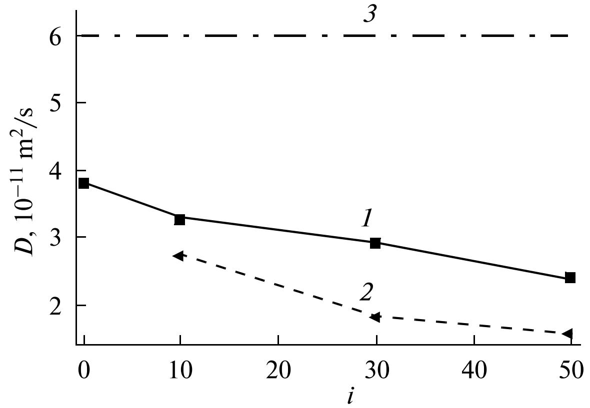

**Fig. 8.** Self-diffusion coefficient in $Ag_i(SiO_2)_{50}$ clusters depending on the number *i* of silver atoms for components: (*1*) $SiO_2$, (*2*) Ag; (*3*) *D* value for the $SiO_2$ structural unit in the $(SiO_2)_{576}$ nanoparticle at 2000 K, MD-calculation [41].

and $\beta_T$ is the isothermal cluster compressibility. The method of the calculation of the $\beta_T$ value is described in [42]. The isodynamic stability coefficient $1/V\beta_T$ for the studied clusters has a maximum value at $i = 30$ (curve *1*, Fig. 7). The values of the $1/V\beta_T$ coefficient for the clusters is lower than that for α-quartz (line *2*) [43] and for crystalline silver (line *3*) [44]. The dependence of the number of electrons $N_{el}$ participating in the interaction with infrared radiation, on the number *i* of the Ag atoms in the cluster has a maximum occurring at $i = 30$ (curve *4*, Fig. 7). The value $N_{el}$ for the cluster with 30 Ag atoms is 1.6 times higher than that of the $(SiO_2)_{50}$ cluster.

The self-diffusion coefficient *D* was determined in terms of the average square of the displacement of atoms (structural units) in the limit of the long times

$$D = \frac{1}{6}\lim_{t\to\theta}[\langle\Delta r^2(t)\rangle/t].$$

The calculated values of the *D* coefficient for the $SiO_2$ structural units and Ag atoms are given in Fig. 8. It is seen that the *D* value for the $SiO_2$ units is noticeably higher than the values of the self-diffusion coefficient of silver atoms. The values of the *D* coefficient decrease with an increase in the number of Ag atoms in the cluster both for $SiO_2$ and Ag. The larger the cluster, the slower its realignment occurs. The *D* value for the $(SiO_2)_{576}$ cluster at $T = 2000$ K simulated by the Born–Huggins–Mayer potential [41] is shown by line *3* in the figure. The *D* value can be calculated in the approximation of the activated diffusion $D = D_0(\Delta E/kT)$, where $\Delta E$ is the activation energy for diffusion. Taking into account the temperature change of the configuration entropy for supercooled $SiO_2$ at 293 K, such a determination gives a much higher value $D$ $(= 8 \times 10^{-10}$ m$^2$/s) [5] than that observed in this work. A similar estimate for the supercooled Ag ($T = 293$ K) leads to an even higher *D* value ($= 7 \times 10^{-8}$ m$^2$/s) [45]. At the same time, the low *D* values (within the range $3 \times 10^{-22}$ to $2 \times 10^{-17}$ m$^2$/s) for crystalline Ag in the temperature interval $540 \le T \le 770$ K were obtained in the experiment [46]. The *D* value for silicate glass in this temperature range is on the order of $10^{-21}$–$10^{-22}$ m$^2$/s [47].

## CONCLUSIONS

The effect of the adsorption of silver atoms on the physical properties of the silica cluster, including the surface tension, was studied in this work. The considered time domain turned out to be quite sufficient for the observation of the structural realignment and calculation of the thermodynamic and kinetic properties. Due to the small size of the system, it is difficult to trace if the AG surface was reconstructed. The adsorbed silver atoms tend to make the cluster sphere-like, whereas the$SiO_2$ structural units are elongated in the inhomogeneous curved film independent of whether there are Ag atoms in their surroundings. As a result of the addition of silver atoms to the silica cluster, the normal and tangential components of the pressure tensor considerably change their own values only in the region of the aggregate surface. Independent of the presence of Ag atoms, the tension surface is inserted into the sphere, approximating the cluster, and it is situated in its direct proximity. The surface tension of the initial unstable silica cluster is negative and takes the positive value already after the adsorption of 10 Ag atoms. The mechanical stability coefficient $1/V\beta_T$ of the cluster has the lowest value in the absence of Ag atoms. The dependence of the $1/V\beta_T$ coefficient on the number of Ag atoms in the cluster correlates with the corresponding dependence of the number of electrons capable of interaction with the external electromagnetic field. The $SiO_2$ structural units are characterized by the higher values of the self-diffusion coefficient than the Ag atoms adsorbed by the cluster in aggregates of the same size. The values of the *D* coefficient decrease with the adsorption of new AG atoms by the cluster.

Thus, the adsorption of silver atoms by the silica cluster reduces the mobility of its structural elements. As a rule, it increases the mechanical stability of the cluster and the number of electrons sensitive to the external electromagnetic field. The last circumstance allows the silica cluster with silver coating to effectively transfer the thermal radiation energy to the surrounding medium.

## ACKNOWLEDGMENTS

The work was supported by the Presidium of the Ural Branch of the Russian Academy of Sciences with the integration project performed in the Ural Branch of the Russian Academy of Sciences and Far East Branch of the Russian Academy of Sciences.

## REFERENCES

1. S. C. Glotzer, M. J. Solomon, and N. A. Kotov, Am. Inst. Chem. Eng. J. **50**, 2978 (2004).
2. C. A. Angel, J. Non-Cryst. Solids **131–133**, 13 (1991).
3. P. Richet, Geochim. Cosmochim. Acta **48**, 471 (1984).
4. R. Bohmer, K. L. Ngai, C. A. Angell, and D. J. Plazek, J. Chem. Phys. **99**, 4201 (1993).
5. I. Saika-Voivod, F. Sciortino, and P. H. Poole, Phys. Rev. E **69**, 041503 (2004).
6. P. Hi. Chakraborty, Mater. Sci. **33**, 2235 (1998).
7. E. Cattaruzza, G. Battaglin, F. Gonella, et al., Appl. Surf. Sci. **247**, 390 (2005).
8. C. Felix, C. Sieber, W. Harbich, et al., Phys. Rev. Lett. **86**, 2992 (2001).
9. G. Sieber, J. Buttet, W. Harbich, et al., Phys. Rev. A **70**, 041201 (2004).
10. M. Hillenkamp, Nanotecnology **18**, 015702 (2007).
11. A. L. Pan, H. G. Zheng, Z. P. Yang, et al., Mater. Res. Bull. **38**, 789 (2003).
12. M. Anija, J. Thomas, N. Singh, et al., Chem. Phys. Lett. **380**, 223 (2003).
13. T. Ikeshoji, G. Torchet, and K. Koga, Eur. Phys. J. D **24**, 211 (2003).
14. Y. Wang, B. Li, Z. Luo, et al., Mater. Res. Symp. Proc. **10172**, 1 (2007).
15. P. J. Sell and A. W. Neumann, Angew. Chem., Int. Ed. Engl. **5**, 299 (1965).
16. K. K. Nanda, Appl. Phys. Lett. **87**, 021909 (2005).
17. C. R. Berry, Phys. Rev. **88**, 596 (1952).
18. T. de Planta, R. Ghez, and F. Piuz, Helv. Phys. Acta **37**, 74 (1964).
19. H. J. Wasserman and J. S. Vermaak, Surf. Sci. **22**, 164 (1970).
20. P. A. Montano, W. Schuhe, B. Tesche, et al., Phys. Rev. B **30**, 672 (1984).
21. K. Hofmeister, S. Thiel, M. Dubiel, and E. Schurig, Appl. Phys. Lett. **70**, 1694 (1997).
22. F. Piuz, Helv. Phys. Acta **37**, 620 (1964).
23. P. Tangney and S. Scandolo, J. Chem. Phys. **117**, 8898 (2002).
24. L. A. Girifalco and V. G. Weizer, Phys. Rev. **114**, 687 (1959).
25. S. Sato, D.-R. Chen, and D. Y. H. Pui, Airosol Air Qual. Res. **7**, 278 (2007).
26. H. L. Lemberg and F. H. Stillinger, J. Chem. Phys. **62**, 1677 (1975).
27. A. Rahman, F. H. Stillinger, and H. L. Lemberg, J. Chem. Phys. **63**, 5223 (1975).
28. H. Saint-Martin, B. Hess, and H. J. C. Berendsen, J. Chem. Phys. **120**, 11133 (2004).
29. A. Le Bail, J. Appl. Crystallogr. **38**, 389 (2005).
30. J. M. Haile, *Molecular Dynamics Simulation. Elementary Methods* (Wiley, New York, 1992).
31. V. H. Kotlyakov, *Problems of Solid State Dynamics and Applied Theory of Gyroscopes* (Nauka, Moscow, 1985) [in Russian].
32. R. Sonnenschein, J. Comp. Phys. **59**, 347 (1985).
33. M. Neumann, J. Chem. Phys. **82**, 5663 (1985).
34. W. B. Bosma, L. E. Fried, and S. Mukamel, J. Chem. Phys. **98**, 4413 (1993).
35. L. D. Landau and E. M. Lifshitz, *Course of Theoretical Physics*, Vol. 8: *Electrodynamics of Continuous Media* (Nauka, Moscow, 1982; Pergamon, New York, 1984), Vol. 8.
36. D. H. Tsai, J. Chem. Phys. **70**, 1375 (1978).
37. S. Ono and S. Kondo, *Molecular Theory of Surface Tension in Liquids* (Springer, Berlin, 1960; Inostr. Liter., Moscow, 1963).
38. F. P. Buff, J. Chem. Phys. **23**, 419 (1955).
39. S. Cuenot, C. Fretigny, S. Demoustier-Champagne, and B. Nysten, Phys. Rev. B **69**, 16510 (2004).
40. M. Dubiel, S. Brunsch, W. Seifert, et al., Eur. Phys. J. D **16**, 229 (2001).
41. L. V. Schweigert, K. E. J. Lehtinen, M. J. Carrier, and M. R. Zachariah, Phys. Rev. B **65**, 235410 (2002).
42. O. A. Novruzova, O. R. Rakhmanova, and A. E. Galashev, Russ. J. Phys. Chem. A **81**, 1825 (2007).
43. L. Levien and C. T. Prewitt, Am. Mineralogist **66**, 324 (1981).
44. Charles Kittel, *Introduction to Solid State Physics* (Nauka, Moscow, 1978; Wiley, New York, 2004).
45. A. V. Gorshkov, Inorg. Mater. **36**, 167 (2000).
46. N. Q. Lam, S. J. Rothman, H. Mehrer, and L. J. Nowicki, Phys. Status Solidi B **57**, 225 (1973).
47. J. D. Kalen, R. S. Boyce, and J. D. Cowley, J. Am. Chem. Soc. **74**, 203 (1991).